International Journal of Biology and Life Sciences
ISSN: 2957-9511 | Vol. 5, No. 2, 2024

Preparation of Bionic Starfish TES-TENG and Utilized in the Treatment of Fasciitis

Yanyan Mu [1], Yili Wei [2], Donghua Zhang [3] and Shaojun Zhang [3, *]

[1] Weihaiwei People's Hospital, Weihai, Shandong, China
[2] Civil Aviation University of China, Tianjin, China
[3] Shandong Jiaotong University, Jinan, Shandong, China

*** Corresponding author:** Shaojun Zhang (Email: dlmu212@163.com)

Abstract: The bionic starfish-designed TES-TENG patch is applied directly to the patient's painful area. During movement, the deformed and fractioned patch generates a pulsed electrical output, which is then converted into an electric field and self-heated by the IDT to treat fasciitis. After TEF-TENG treatment, the total clinical effectiveness rate of the observation group was 94.54%, which was higher than that of the control group (75.83%), suggesting that TEF-TENG could enhance the clinical efficacy of the basic rehabilitation training. The self-powered TES-TENG, stimulates the nodules on the attachment points of the sacral spine or iliac crest muscles through external physical stimulation, repairs the tissue fibrosis that occurs after damage to the fascia, and enhances the proliferation and migration of fibroblasts in order to promote the dissipation of the nodules, while the TES-TENG synergistically utilizes the antiseptic, sensory properties, and heating properties to alleviate the pain.

Keywords: Bionic Starfish TES-TENG; Fasciitis; Reduce Patient Pain; Fasciitis Treatment.

1. Introduction

In the medical field, uninterruptible power supply has been a significant obstacle, and existing battery technologies have many drawbacks, comparing bulky size, limited capacity and shelf life, and costs associated with surgical-based battery recharging. The emergence of TENGs, which offer a new method of converting the biomechanical energy of living organisms into electrical energy, is attracting a lot of attention as they have excellent prospects for medical applications ranging from bio-monitoring to therapeutics. These self-powered nanogenerators enable devices to operate autonomously by harnessing the minute mechanical movements of internal organs such as heartbeat, respiration, blood circulation, muscle contraction/dilatation, and lung vibration. TENGs are typically found in thin film form and utilize the synergistic effect of triboelectric and electrostatic induction effects to produce a periodic electrical output. Self-powered technologies include implantable piezoelectric nanogenerators and implantable triboelectric nanogenerators due to the significant advantages of TENGs such as their light weight, membrane-like structure, flexibility, and ability to be self-powered. Due to their inherent flexibility and self-powered nature, they can be used in drug delivery, muscle stimulation, tissue regeneration and adjunctive therapies [1] Implantable devices are used in a wide range of sensing applications in a variety of fields including cardiac, gastrointestinal, bladder and ligamentous strain monitoring. therapeutic applications for IBDs such as neurostimulation, bone stimulation, cartilage therapy, tissue regeneration, muscle stimulation, drug delivery, and diabetes management [2]. For example, the implantation of neural prostheses and thus restoration of touch in some patients with traumatic peripheral nerve injuries or soft tissue loss with loss of sense of touch is a promising direction. Iftach Shlomy et al. (2021) at Tel Aviv University manufactured and demonstrated a friction TENG integrated haptic device, TENG-IT, implanted under the skin [3]. Tests showed that TENG-IT implantation provided tactile ability without interfering with the rat's locomotor ability, and this study makes TENG-based self-powered implantable devices tremendously promising as a means of restoring tactile sensation. Tao Song et al. (2023), in order to achieve wide operating temperatures and multi-parameter body motion sensing using TENG sensors, prepared a 3D-printing based preparation of a functionalized heat-resistant TENG sensor [4], the functionalized TENG sensor and human-machine interface were printed and subsequently networked on the human body to sense comprehensive motion information. The results show that six typical motions can be recognized with 94.85% accuracy based on a neural network algorithm. In addition, a simple digital twin for motion capture and trajectory tracking in virtual space has been implemented, combining the proposed TENG sensor with a virtual reality (VR) platform, opening a new path for human safety monitoring in hot environments.

For the application of TENGs in sustainable energy generation and wearable medical monitoring systems, the development of TENG monitoring has been a hot research topic in recent years. Joon-Ha Son et al. (2023) developed the BB-TENG aimed at harvesting kinetic energy from human movement [5]. Meiru Mao (2024) reported that MXene-based TENG for wound-healing accelerated Study [6], TESP combined with near-infrared photothermal effect to promote wound healing and acted as a real-time monitoring sensor for physiological signals. B. Indumathy et al. (2024) based on electrospun PVDF/silane-based hyperbranched polyester third-generation nanofibre mesh blends [7]. B. Indumathy et al. (2024) based on electropunk PVDF/silane-based hyperbranched polyester third-generation nanofiber mesh blends Shuhong Huang et al. (2024) proposed a strategy to utilize the synergistic effect of polydopamine-coated cerium oxide (CeO2@PDA) nanoparticles and polyvinylidene difluoride (PVDF) to fabricate multifunctional and flexible textiles (PCPs) [8]. Sen Li et al. (2024) developed a novel tactile perception system based on friction electrical sensors [9], the system has the added functionality of quantum rods.

Junyi Yin et al. (2024) investigated a variety of TENG-based wearable sensors [10], which have demonstrated applications in the field of eye-movement monitoring and wider human-computer interaction. Jaehyeok Shin et al. (2024) developed self-powered flexible piezoelectric motion sensors (PMSs) with InN NWs as the response medium [11], spatially controlling the arrangement of InN NWs by applying a magnetic field.

In 2023, clinical practice guidelines from the American College of Physicians and the U.S. Department of Defense indicated that most patients do not require surgery, and that conservative treatments such as rehabilitation, acupuncture, tui-na, exercise, scalding, medications, and electrical stimulation are sufficient to achieve the desired therapeutic effect. Recent studies have found that direct current electrical stimulation (ES) has great potential to promote cellular movement, stimulate collagen production and promote successful wound healing [12]. Human movement generates piezoelectricity, which in turn generates additional bioelectrical signals. Bioelectrical stimulation promotes the differentiation and proliferation of stem cells in tissues such as tendons and ligaments, which in turn dissipates nodules, inhibits local inflammation, and activates regenerative pathways in the my-ofilm. However, the biggest disadvantage of electrical stimulation therapy is that it requires an external power supply, and the external power supply of electrical stimulation devices is usually bulky and heavy, which brings inconvenience to treatment and rehabilitation. Therefore applying ES to mobile and wearable devices is innovative and challenging. Current research on myo-fasciitis is mostly based on clinical efficacy observation, and the mechanism of pain modelling for the treatment of myofascial inflammation has not yet been clarified. Qianying Liu et al. (2024) applied a quantitative sensory nerve detector to quantitatively evaluate pain changes before and after treatment [13]. Elastic ultrasound quantifies whether the elasticity of fascia is reduced by scoring the elasticity image of the fascia and calculating the strain rate relative to the surrounding soft tissues. However, there was no expert consensus on quantifying pain and efficacy evaluation, and the scales were mostly judged by patients' subjective sensations, with the risk of data bias, which urgently needs to be quantified to enhance the credibility of the evidence. It is the focus of future research to validate the mechanisms of these external TCM treatments through research and to safely and effectively transform them into precise treatments or drugs. Self-powered TES-TENG can greatly improve the tissue fibrosis that occurs after fascial damage. TENGs are applied to enhance the proliferation and migration of fibroblasts to promote the dissipation of nodules; the use of TENG as a self-powered electronic device for the treatment of fasciitis when it is used as a power source is a novel exploration.

2. Experimental Materials and Methods

2.1. Preparation of PDMS@TiO_2 Membrane

The cut PMMA substrate was subjected to surface treatment, and toluene was used as the solvent, 100 mL of toluene solution was taken, 400 μL of octadecyltrichlorosilane (OTS) was added, and the mixture was homogeneously mixed and poured into a glass petri dish, and then the substrate was cleaned by anhydrous ethanol, and poured into an ultrasonic cleaner of deionized water, respectively, and nitrogen was blown dry, and then placed into the OTS toluene solution to carry out molecular self-assembly treatment. After 30 s, the substrate was removed and the residual OTS was cleaned with toluene solution. The surface energy of the treated substrate was reduced, which made it easier for the subsequent PDMS preparation to uncover the film. The mixture was pumped using a vacuum pump for a duration of 10 min, during which the pressure was maintained at 2×10^{-3} MPa, to ensure that the air bubbles in the PDMS were completely discharged. Subsequently, it was placed on the coating machine for coating, with a coating rate of 0.5 mm/s, and horizontally coated for 2 min, coated onto the high-temperature-resistant toughened glass plate, and then put into a vacuum drying oven to dry at 60°C for 30 min, and the film was peeled off from the high-temperature-resistant toughened glass plate after completion of the drying process. The addition of TiO_2 nanoparticles to the PDMS matrix improves the corrosion ability of the material. TiO_2 with mass fractions was taken and added to the PDMS prepolymer, and the mixed solution was placed in the centrifugal tank of a vacuum centrifugal mixer and vacuum centrifuged and stirred for 15 min, to make a 2 wt% PDMS@TiO_2 solution. After drying by coating, a 2 wt% PDMS@TiO2 film was made, and 4 wt%, 6 wt%, and 8 wt% solutions were obtained in the same way and cured to form a film. Finally, the PDMS membrane was peeled off the silicon template to produce the microporous array membrane.

2.2. Preparation of Copper Electrode Layer

Copper foil was selected as the electrode layer in the TES-TENG device. The Cu electrode was sanded using 400-grit sandpaper to remove the oxide layer on the surface. After that, the Cu electrode was put into an ultrasonic cleaner and washed first with acetone, then with ethanol and deionized water respectively to remove the pollutants on the surface of the Cu electrode, and finally dried naturally in a pollution-free environment.

2.3. TES-TENG Preparation

The friction layer substrate and device shell, 2.5 mm thick acrylic plate cut into 100 mm × 100 mm, 130 mm × 130 mm each of six pieces and keep the surface clean. The produced copper foil and PDMS friction layer are pasted on one surface of each acrylic plate in turn, of which only copper foil is pasted on the 130 mm × 130 mm acrylic plate, copper foil and PDMS friction layer are pasted on the 100 mm × 100 mm acrylic plate, and the PDMS friction layer is coated on top of the copper foil. Then 6 pieces of 100 mm×100 mm acrylic plates and 6 pieces of 130 mm×130 mm acrylic plates were bonded into cubes, and the 8 vertices of the 100 mm cube and the vertices of the 130 mm cube were connected with elastic cords during the bonding process.

3. Results and Discussion

3.1. SEM Morphology Analysis

The microscopic morphology of PDMS@ TiO_2 nanocomposite membranes doped with different concentrations of TiO_2 nanoparticles was observed using a Sigma 300 scanning electron microscope (SEM) from Zeiss, Germany, and the specific results are shown in Figure 1. Among them, the surface of pure PDMS membrane is relatively smooth without any particle doping and air bubbles; while the surface of the nanocomposite membrane with different concentrations of TiO_2 nanoparticles added becomes rough and there are a lot of white granular substances, which is due to the doping and loading of TiO_2 nanoparticles on the surface; and with the increase of TiO_2 nanoparticles doping concentration, the surface roughness of nanocomposite film becomes larger and this granular material is more and more obvious, which proves that the doping of TiO_2 nanoparticles affects the surface morphology of the PDMS membrane. The particulate matter in the nanocomposite membrane causes its surface to become rough, and this process increases the specific surface area of the membrane. Its surface properties help to enhance the contact effect between the friction electric materials, thus enhancing the electrical output performance of the friction dielectric materials.

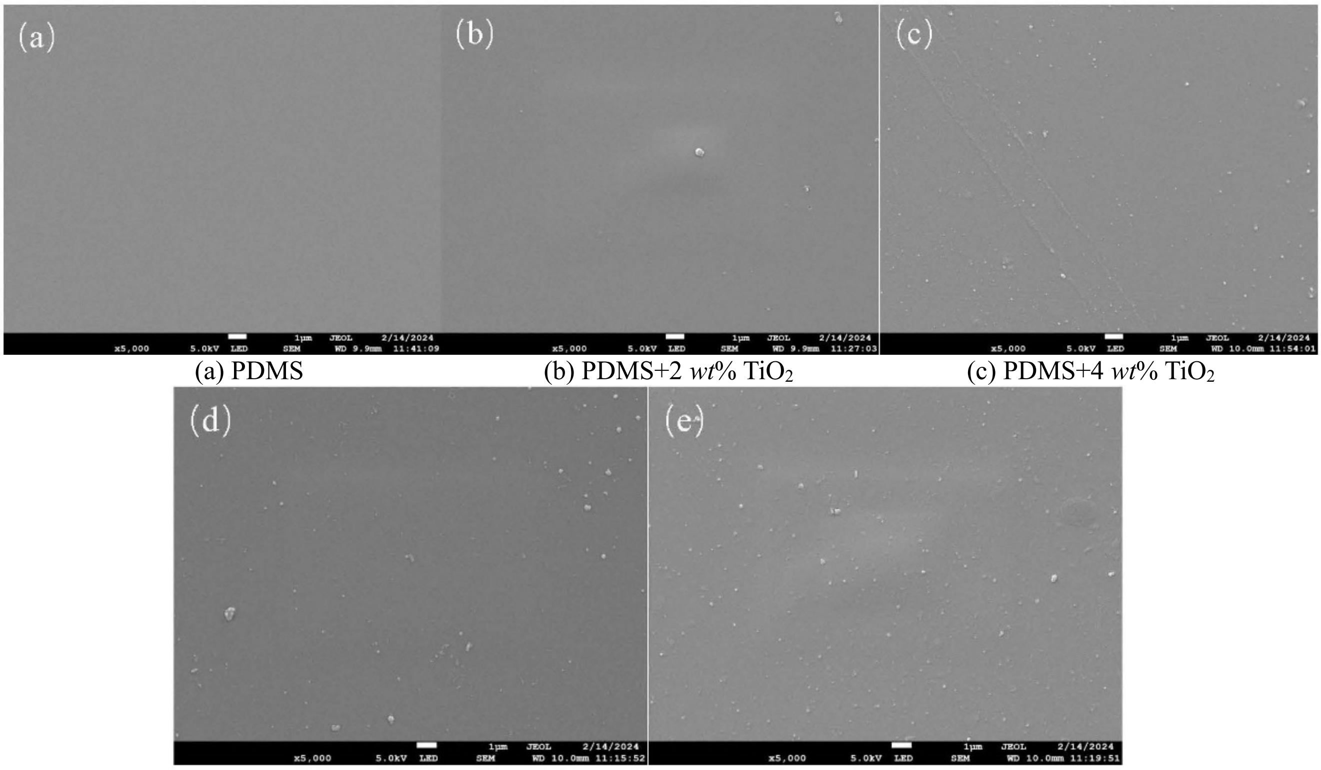

(a) PDMS (b) PDMS+2 *wt*% TiO_2 (c) PDMS+4 *wt*% TiO_2

(d) PDMS+6 *wt*% TiO_2 (e) PDMS+8 *wt*% TiO_2

Fig 1. SEM images of PDMS membranes with different TiO_2 doping concentrations

3.2. Infrared Spectral Analysis

In order to deeply investigate the chemical structure of the specimens and how the doping amount of TiO_2 nanoparticles affects the chemical composition of the specimens, the pure PDMS film as well as the PDMS@TiO_2 composite nanofilms with different TiO_2 doping concentrations were analyzed by Fourier transform infrared spectroscopy (FTIR) in this study. As shown in Fig.2, the 1# curve represents the infrared spectral curve of the pure PDMS membrane, while the 2#, 3# and 4# curves correspond to the spectra of the PDMS@TiO_2 composite membranes with different concentrations. Comparing with the 1# curve, no significant changes in the positions of the characteristic absorption peaks were observed for the 2#, 3# and 4# curves, indicating that the doping of TiO_2 did not significantly change the chemical structure of the composite film, while the appearance of TiO_2 broad characteristic absorption peaks at 1450-1300 cm^{-1} indicates that TiO_2 is present in the PDMS film. Among them, the characteristic absorption peaks at 2905 cm^{-1} and 1895 cm^{-1} of the 4 wt% PDMS@ TiO_2 film were significantly weakened compared to the other films, which indicated that the increase of TiO_2 made the content of $-CH_3$ and Si-O-Si groups in the PDMS decrease, hydrophilicity weakened, and hydrophobicity increased, which was in agreement with the results of the contact angle experiments.

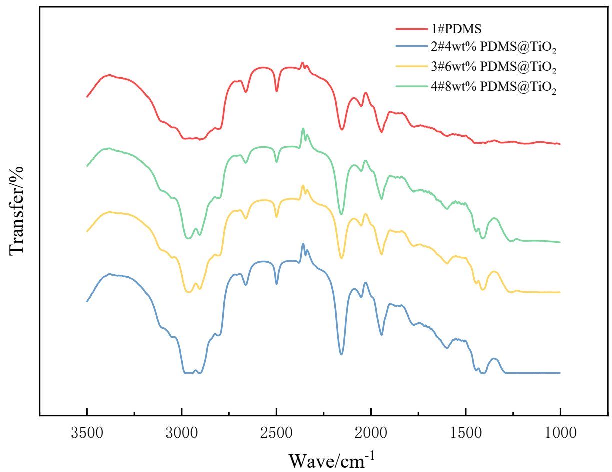

Fig 2. Infrared spectra of PDMS films with different TiO_2 doping concentrations

3.3. Friction Layer Output Performance

In order to evaluate the electrical output performance of TENGs made by combining PDMS@TiO_2 nanocomposite films containing different mass fractions of TiO_2 nanoparticles with Cu foils and PMMA plates, the electrical properties were tested separately. The open-circuit voltage of the pure PDMS-based friction nanogenerator was 45.25 V and the short-circuit current was 5.35 μA. The output electrical performance of the TiO_2 nanoparticles doped TENGs was significantly improved compared to the pure PDMS-based friction nanogenerator due to the fact that the relative permittivity of PDMS nanocomposite film would be increased by the addition of TiO_2 nanoparticles, which would result in an effective enhancement of dielectric properties. In the measured experiments, the electrical performance of the friction nanogenerator reaches the best when the doping mass fraction of TiO_2 nanoparticles is 4 wt%, and its maximum open-circuit voltage can reach 72.85 V, and the maximum short-circuit current is 7.89 μA, which are 1.6 times and 1.8 times higher than the open-circuit voltage and short-circuit current of the undoped titanium dioxide nanoparticles of the pure PDMS film, respectively. Therefore, the PDMS@TiO_2 nanocomposite film with a doping mass fraction of 4 wt% was selected for the performance study of the friction nanogenerator in the subsequent experiments.

3.4. Effect of Amplitude on TES-TENG Output Performance

The effect of amplitude on the power generation performance of TES-TENG (Fig. 3). A linear motor was used to simulate the wave amplitude by changing the stroke of the motor with a frequency parameter of 1.8 Hz, and the amplitude of the test was varied from 20 mm to 125 mm, and the test was carried out one after another at intervals of 15 mm, with the amplitudes of 20 mm, 35 mm, 50 mm, 65 mm, 80 mm, 95 mm, 110 mm, and 125 mm, respectively. During the process of amplitude expansion from 20 mm to 125 mm, the short-circuit current and open-circuit voltage outputs of the TES-TENG show a general trend of increasing with the increase of the external driving amplitude. The short-circuit current increases from 4.15 μA at an amplitude of 20 mm to 10.21 μA at an amplitude of 125 mm, and the open-circuit voltage increases from 53.05 V to 86.01 V. The increased contact area and fuller friction action improved the energy conversion efficiency, which led to the enhanced output performance. Analysis of the experimental data shows that during the amplitude increase, when the motion between the bicubic reaches resonance with the wave, the short-circuit current *I*SC reaches its maximum value at this time and no longer rises indefinitely. Therefore, the TES-TENG can operate effectively under common wave amplitude conditions.

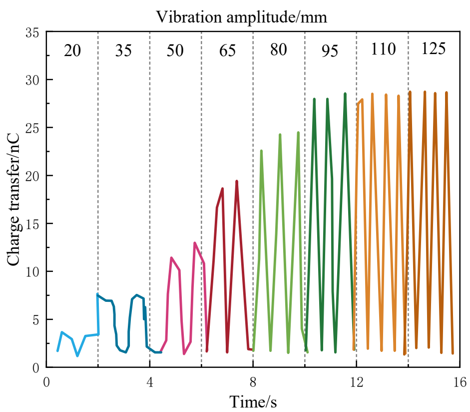

Fig 3. Transferred charge of TES-TENG at different amplitudes

3.5. Effect of Anode Material on Anti-Inflammatory Properties

Carbon rods exhibited the highest bactericidal efficiency among the anode materials at an external driving frequency of 1.8 Hz, achieving 92.85% inactivation at 15 min. When carbon plate was the anode, the inactivation rate was 90.35% at 15 min and increased to 93.55% at 20 min. The bactericidal effect of carbon fibre was lower than the previous two, with an inactivation rate of 84.56% at 15 min and reaching 89.22% at 50 min. After evaluating the bactericidal ability of the three anode materials, carbon rods, carbon plates and carbon fibres, the results showed that carbon rods had the most significant bactericidal effect, and carbon plates were slightly lower than carbon rods. Considering that carbon fibre showed poor bactericidal effect in comparison with carbon plate, and that carbon plate has a significant advantage in terms of cost and effective area (relative to the same volume of carbon rod), based on this, carbon plate was used as the target material for the next experimental study.

3.6. Effect of Frequency on Sterilization Performance

Under the frequencies of 1.0 Hz, 1.2 Hz, 1.4 Hz and 1.6 Hz, the overall trend of the sterilization performance increased with time, and the higher the frequency, the greater the sterilization rates (SR) were in relative terms. Under the effect of 1.6 Hz frequency, the SR increased rapidly from 72.78% at 10 min to 94.89% at 40 min. And when the frequency was reduced to 1.4 Hz, in contrast, the SR increased slower at the initial stage, 65.25% at 10 min of electrolysis, and reached 93.12% SR after 40 min of electrolysis. At 1.2 Hz and 1.0 Hz, the SR increased more slowly in the initial stage, and after 40 min of electrolysis, 84.36% and 44.63% SR were achieved, respectively. It was analyzed and concluded that the poor output performance of TES-TENG at these two frequencies made the initial oxidation potential of the anode lower than that of chloride ions, thus failing to generate chlorine gas, resulting in a low sterilization efficiency at the initial stage. However, with the gradual accumulation of the surface charge of TES-TENG, its output performance was improved, and the anodic potential eventually exceeded the oxidation potential of chlorine ions, and chlorine gas began to be generated, thus demonstrating the sterilization effect.

3.7. Comparison of Clinical Outcomes After Treatment Between the Two Groups of Patients

As seen in table 1, after clinical treatment, the total clinical effective rate of the observation group was 94.54%, which was higher than that of the control group (75.83%, $P < 0.01$). Comparison of TCM evidence scores before and after treatment between the two groups of patients. Before treatment, there was no statistically significant difference between the TCM evidence scores of the two groups ($P > 0.05$); after treatment, the TCM evidence scores of both groups were lower than those before treatment ($P < 0.05$), and the observation group was lower than the control group ($P < 0.05$).

Table 1. Comparison of clinical efficacy between the two groups [Case (%)].

Group	Number of cases	Clinical cure	Significant	Effective	Ineffective	Total Effective
Observation group	110	26(23.63)	46(41.82)	32(29.09)	6(5.45)	104(94.54)
Control group	120	15(12.50)	37(30.83)	39(24.17)	29(34.16)	91(75.83)

4. Conclusion

After TEF-TENG treatment, the total clinical effectiveness rate of the observation group was 94.54%, which was higher than that of the control group (75.83%), suggesting that TEF-TENG could enhance the clinical efficacy of the basic rehabilitation training. In addition, the TCM evidence scores of both groups after treatment were lower than those before treatment, and the observation group was lower than the control group, the difference was statistically significant ($P < 0.05$), which also indicated that TEF-TENG could effectively improve inflammation. In addition, the ODI, RMDQ, and VAS scores of both groups improved after treatment ($P < 0.05$), and the efficacy of each index in the observation group was better than that in the control group ($P < 0.05$, $P < 0.01$), which further proved that this formula could effectively improve the lumbar dysfunction and pain caused by inflammation. Improve the quality of life of patients. This study provides a certain reference for clinical treatment of TF. Although TENG has made great progress in the treatment of pain, there are still some issues that need to be resolved for the future development of this research field:(1) Improving the output energy of TENG: From the inside, many studies nowadays enhance the contact proximity by modifying the material or creating surface micro- and nano-structures to increase the surface charge density. Externally, the working environment can be optimized by introducing power management circuits, e.g. charge pumping and self-charging excitation are 2 newly developed effective mechanisms to increase the output power of TENGs. (2) Improve the durability of materials and equipment: Long-term stability is a key issue in the practical application of TENGs, and the wear and tear of materials during use will lead to performance degradation. Output performance and durability can be improved by designing contact and non-contact switching, or through the introduction of new materials. (3) Reducing the impact of TENG materials on the environment: most of the materials for TENG are non-biodegradable synthetic polymers, which may cause environmental pollution, biodegradable and renewable materials, however, tend to have insufficient friction electrical and mechanical properties, and the exploration of natural materials requires further research to improve. (4) Effective energy storage of TENG: Conventional energy storage devices are usually charged using DC input. In view of the pulse output characteristics of TENG, it is important to study the transport and diffusion of ions on the isolation film under the action of pulse driving force in lithium batteries, which will further expand the scope of application of TENG.

References

[1] Akshpreet Kaur, Ankur Gupta, Cuifeng Ying et al. Smart wearable triboelectric nanogenerator for self-powered bioelectronics and therapeutics, Microelectronic Engineering, 2023, 275, 111992.

[2] Arshad Khan, Ravindra Joshi, Manish Kumar Sharma et al. Piezoelectric and triboelectric nanogenerators: Promising technologies for self-powered implantable biomedical devices, Nano Energy, 2024, 119, 109051.

[3] Shlomy, Iftach, et al. Restoring tactile sensation using a triboelectric nanogenerator. ACS nano 2021, 15(7): 11087-11098.

[4] Tao Song, Saihua Jiang, Nixin Cai, Guohua Chen et al. A strategy for human safety monitoring in high-temperature environments by 3D-printed heat-resistant TENG sensors, Chemical Engineering Journal, 2023, 475, 146292.

[5] Joon-Ha Son, Weon-Guk Kim, Seong-Yun Yun et al. Wearable bead-based triboelectric nanogenerator with dual-mode operation for monitoring abnormal behavior in dementia patients, Nano Energy, 2023, 114, 108642.

[6] Meiru Mao, Jianglong Kong, Xiaohan Ge et al. Mxene-based wearable self-powered and photothermal triboelectric nanogenerator patches for wound healing acceleration and tactile sensing, Chemical Engineering Journal, 2024, 482, 148949.

[7] Kumar Shrestha, Gagan Bahadur Pradhan, Trilochan Bhatta et al. Intermediate nanofibrous charge trapping layer-based wearable triboelectric self-powered sensor for human activity recognition and user identification, Nano Energy, 2023, 108, 108180.

[8] Shuhong Huang, Xiaohui Zhao, Chenlong Hao et al. Multifunctional PVDF/CeO2@PDA nanofiber textiles with piezoelectric and piezo-phototronic properties for self-powered piezoelectric sensor and photodetector, Chemical Engineering Journal, 2024, 482, 14895.

[9] Sen Li, Yu Cheng, Ka Deng, Hongyan Sun et al. A self-powered flexible tactile sensor utilizing chemical battery reactions to detect static and dynamic stimuli, Nano Energy, 2024, 124, 109461.

[10] Junyi Yin, Vishesh Kashyap, Shaolei Wang et al. Self-powered eye-computer interaction via a triboelectric nanogenerator, Device, 2024, 2(1), 100252.

[11] Jaehyeok Shin, Siyun Noh, Jinseong Lee et al. Self-powered flexible piezoelectric motion sensor with spatially aligned InN nanowires, Chemical Engineering Journal, 2024, 486, 150205

[12] Yifan Wu, Kaihang Zhang, Sihao Li et al. Self-powered wearable electrical stimulation patch with integrated triboelectric nanogenerator for tendinopathy treatment, Nano Energy, 2024, 121, 109234.

[13] Qianying Liu, Yuenan Liu, Jiazhen Zhang et al. Gut microbiota deficiency aggravates arsenic-induced toxicity by affecting bioaccumulation and biotransformation in C57BL/6J mice, Food and Chemical Toxicology, 2024, 186, 114564.